Nanoscale

Accepted Manuscript

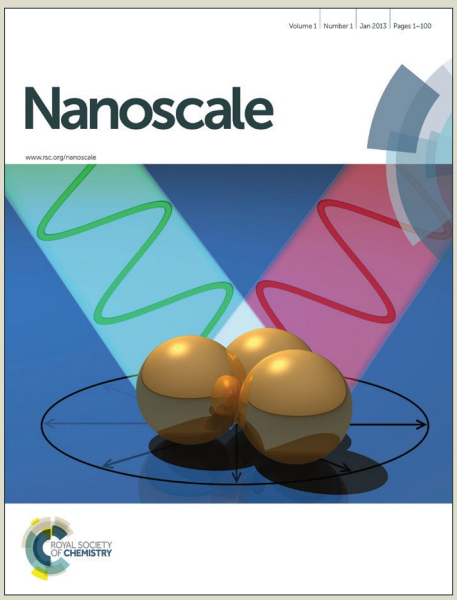

ROYAL SOCIETY OF CHEMISTRY

www.rsc.org/nanoscale

Dopant type and amount governs the electrochemical performance of graphene platforms for the antioxidant activity quantification

Kai Hwee Hui, Adriano Ambrosi, Zdeněk Sofer, Martin Pumera, Alessandra Bonanni*

Division of Chemistry & Biological Chemistry, School of Physical and Mathematical Sciences, Nanyang Technological University, Singapore 637371

Fax: (65) 6791-1961

Email: a.bonanni@ntu.edu.sg

*Author for correspondence

Abstract

Graphene doped with heteroatoms can show new or improved properties as compared to the original undoped material. It has been reported that the type of heteroatom and the doping conditions can have strong influence on the electronic and electrochemical properties of the resulting material. Here we wish to compare the electrochemical behavior of two n-type and two p-type doped graphenes, namely boron-doped graphenes and nitrogen-doped graphenes containing different amounts of heteroatom. We show that the boron-doped graphene containing the higher amount of dopant provides the best electroanalytical performance in terms of calibration sensitivity, selectivity and linearity of response for the detection of gallic acid normally used as standard probe for the quantification of antioxidant activity of food and beverages. Our findings demonstrate that the type and amount of heteroatom used for the doping have a profound influence on the electrochemical detection of gallic acid rather than the structural properties of the material such as amounts of defects, oxygen functionalities and surface area. This finding has a profound influence on the application of doped graphenes in analytical chemistry field.

Introduction

Heteroatom-doped graphene materials have been drawn the interest of the scientific community due to their improved physicochemical, optical, electromagnetic and structural properties, as compared to undoped graphenes.[1-3] Recent reports demonstrated that different electronic properties are shown by p- and n-type doped graphenes obtained by performing the doping with either electron donating or withdrawing species.[4-6] It was also reported that, depending on the precursor and the experimental conditions used for the doping, it is possible to tune the doping efficiency and control the heteroatom distribution and configuration in the original graphene structure.[7-10]

Thus far, the properties of different p- and n-type doped graphenes obtained with various procedures and presenting diverse amount of heteroatom have been evaluated for several applications including supercapacitors,[11] fuel and solar cells,[12] electrocatalysis for oxygen reduction reaction[13-17] and electronics[2, 4]. However, little has been done on the investigation of electrochemical properties[18] of those materials and the effect of different doping precursor and conditions towards the detection of various electrochemical probes. It is indeed expected that graphene material doped with electron donating heteroatoms would show a diverse electrochemical behavior as compared to those doped with electron withdrawing heteroatoms. The dissimilar behavior may also depend on the doping mode, being the difference between p-type and n-type doped graphene more obvious when substitutional doping occurs.[10]

In this work we produced p- and n-type doped graphenes by thermal exfoliation of graphite oxide at different temperature. Boron-doped graphene was produced in the presence of BF_3 as boron precursor, while nitrogen-doped graphene was produced in the presence of NH_3 as nitrogen precursor.[19] For both materials thermal exfoliation was carried out at two different temperatures of 800°C and 1000°C in order to tune the doping efficiency. Figure 1 shows a scheme for the synthesis of undoped, boron-doped and nitrogen-doped thermally reduced graphene materials (B-TRG and N-TRG). All graphene materials were employed for the electrochemical detection of gallic acid, a

standard probe that is commonly used for the evaluation of antioxidant properties of food and beverages due to polyphenol content in them.

We report here that surprisingly, the electrochemical performance of B- and N-doped graphene towards the detection of gallic acid is governed on the type and amount of heteroatom and not on the structural properties of the materials such as amounts of defects, oxygen functionalities and surface area.

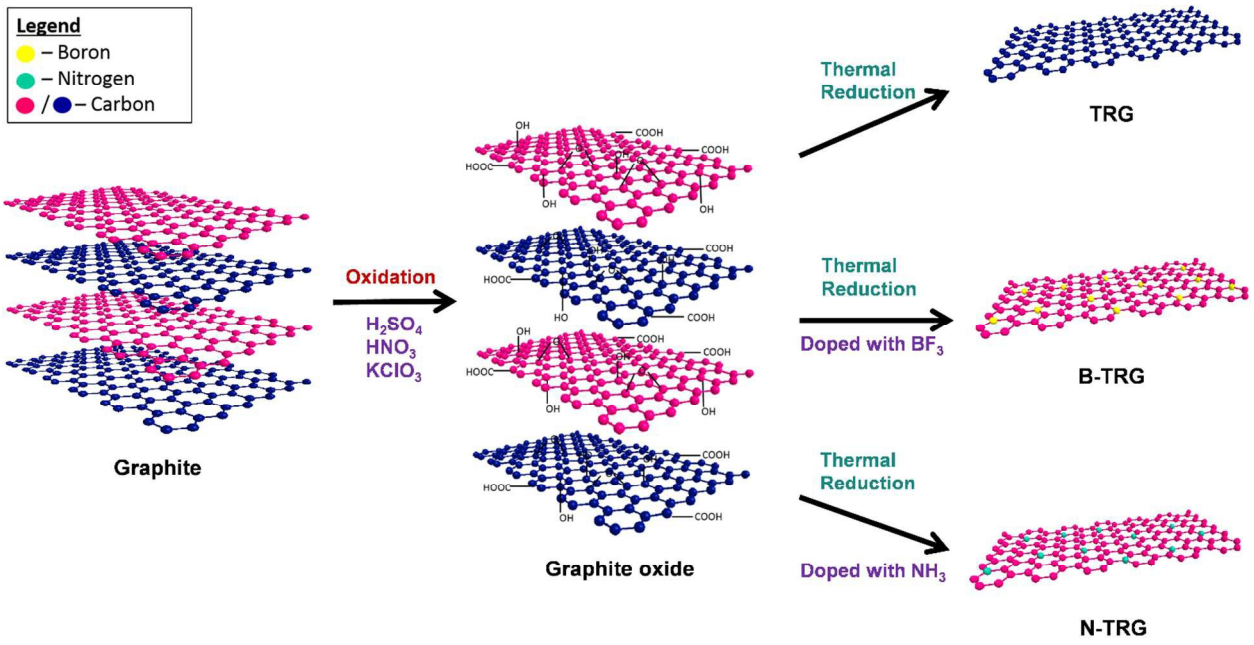

Figure 1. Schematic representation of the synthesis of undoped (TRG), boron-doped (B-TRG) and nitrogen-doped (N-TRG) thermally reduced graphene materials.

Results and discussion

Heteroatom-doped graphene used in this study were prepared by thermal exfoliation of graphite oxide at 800°C and 1000°C either in the presence of BF_3 or NH_3 as the heteroatom precursor. It was previously demonstrated that both the doping efficiency

and the bonding configuration are influenced by the employed temperature.[1] At the temperatures of 800°C and 1000°C employed in this work the formation of B-C bonding and N-C bonding due to substitutional doping is expected in the doped graphene.[7, 20] Prompt gamma-activation analysis revealed that the concentration of boron within graphene was 140 ppm for exfoliation performed at 800°C (B-TRG-L), and 590 ppm for exfoliation performed at 1000 °C (B-TRG-H). From the combustible elemental analysis, the nitrogen content was calculated to be 1.9 % for exfoliation performed at 800°C (N-TRG-L), and 2.2 % for exfoliation performed at 1000°C (N-TRG-H) respectively. Table 1 shows the results obtained from the further characterization of the materials by Raman spectroscopy, X-ray photoelectron spectroscopy and for the measurement of the surface area by the Brunauer-Emmett-Teller (BET) method (please refer to Figure S1 and Figure S2 in *Supporting Information* for the characterization spectra). The boron was not detected by XPS at 190 eV due to low doping level (note that the detection limit of XPS is ~0.1 atom %), whilst clear signal for nitrogen was recorded around 400 eV confirming the presence of pyrrolic and quaternary nitrogen in the graphene network.[19]

Table 1. Material characterization by prompt gamma-activation analysis, elemental analysis, Raman spectroscopy, XPS, and BET.[19] (H) and (L) indicate higher and lower dopant content, respectively.

Material	Amount of dopant	D/G ratio	C/O ratio	Surface area (m^2/g)
TRG (undoped)	-	0.91	8.6	109
B-TRG-H	590 ppm	0.75	16.8	34
B-TRG-L	140 ppm	0.70	8.6	142
N-TRG-H	2.2 wt %	0.70	15.8	57
N-TRG-L	1.9 wt %	0.46	20.7	98

Comparative voltammetric analysis of gallic acid oxidation on undoped thermally reduced graphene exfoliated at 1000°C (TRG), B-doped thermally reduced graphene exfoliated at 1000°C (B-TRG-H) and 800°C (B-TRG-L), and N-doped thermally reduced

graphene exfoliated at 1000°C (N-TRG-H) and 800 °C (N-TRG-L) were carried out, as depicted in Figure 2.

Figure 2A shows representative differential pulse voltammograms recorded for gallic acid oxidation on different materials. Among all TRG materials, it can be clearly observed that the oxidation potential recorded using the undoped TRG is higher than that of the doped TRGs. It seems clear that the presence of heteroatoms (boron or nitrogen) within the graphene lattice can facilitate the electron transfer between gallic acid and the electrode surface, which occurs at lower potentials on doped graphene surfaces. The second aspect to keep into consideration is represented by the sensitivity, which can be evaluated by measuring the peak current intensity using the same amount of graphene material. It can be seen in Figure 2B, that the TRG modified electrodes showed significantly higher peak current than the bare GC electrode, which can be attributed to the fact that TRGs have more structural defects and thus greater electroactive surface area than GC.[21] Comparing the TRGs, the oxidation current increased in the order: N-TRG-L < TRG < N-TRG-H < B-TRG-L < B-TRG-H. Interestingly, this result is inconsistent with the level of structural defects which follow the trend: N-TRG-L < B-TRG-L ≈ N-TRG-H < B-TRG-H < TRG, from the lowest to highest D/G ratio as summarized in Table 1 from Raman spectroscopy characterization. It appears that the presence of structural disorders and defects does not have significant effect on the sensing capacity of the graphene material towards the detection of gallic acid, since the undoped TRG, having the largest density of defects, did not display the largest current response. Different surface areas of the materials, measured by the Brunauer-Emmett-Teller (BET) method, were also kept into consideration confirming once again the superior performance of the boron-doped materials.

In order to provide further insight into the electrochemical behavior of the analyzed materials a scan rate study was carried out to calculate the electroactive surface areas of GC, TRG, B-TRG-L, B-TRG-H, N-TRG-L, and N-TRG-H. Figure S3 shows the peak current relative to the electroactive surface area for each material. From the figure it is clear that the results obtained for the electrochemical signal of B-TRG-L, N-TRG-L, and N-TRG-H is indeed due to the different electroactive surface area. As for the B-TRG-H,

the largest electroactive surface area alone cannot explain the best analytical performance, which can be actually due to the thermodynamically favorable electron transfer between gallic acid and the doped graphene because of the interactions between the electron withdrawing boron and the electron-donating oxygen atoms in gallic acid. This is also confirmed by the larger signal obtained with B-TRG-H as compared to B-TRG-L with lower boron content,[19] which suggests the active role of boron atoms to the oxidative process. Overall, it can be deduced that the type and amount of doping heteroatom dominates the electrochemical behavior of the graphene materials towards the oxidation of gallic acid.

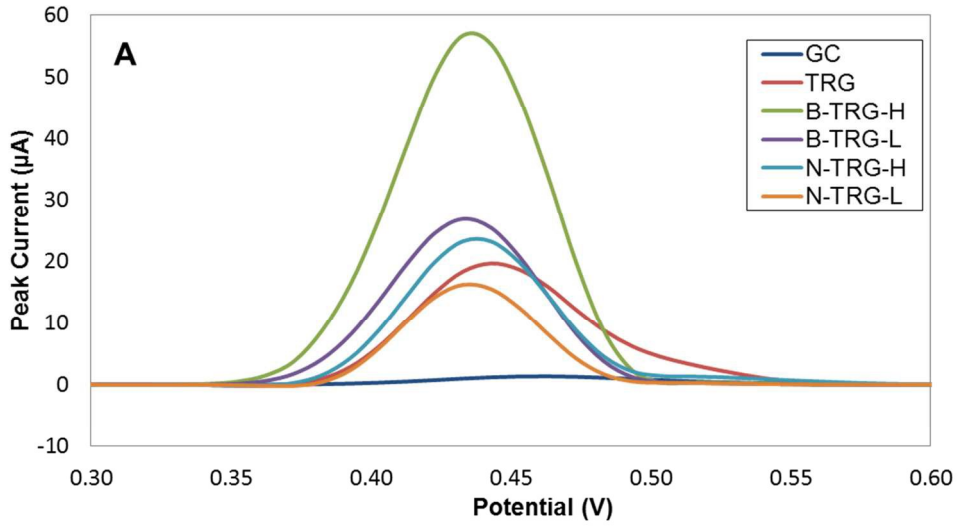

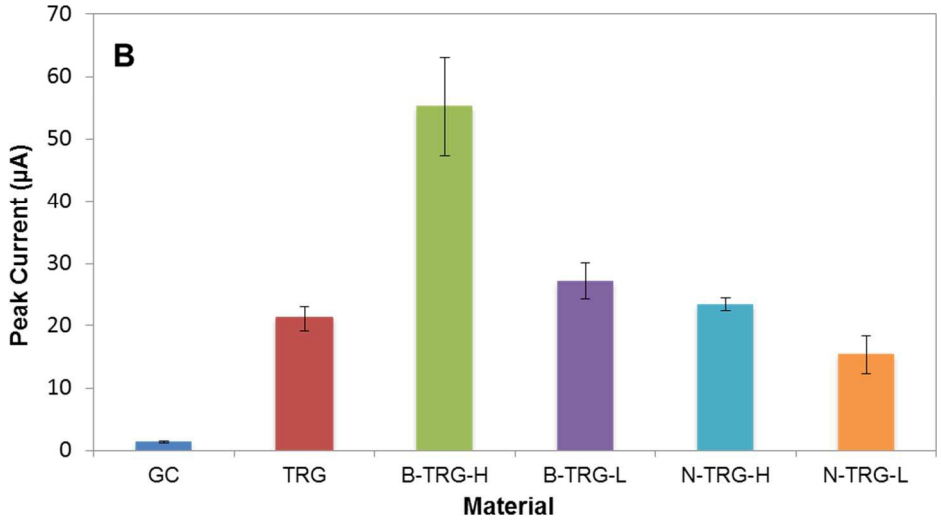

Figure 2. (A) Differential pulse voltammograms of 0.1 mM gallic acid on glassy carbon (GC) and TRG materials. (B) Bar chart of peak current vs material. Conditions: 0.1 M phosphate buffer solution, pH 2.5.

For a detailed assessment on the performance of the TRGs, further investigations on the calibration sensitivity, linearity of response and selectivity of the materials were conducted. Figure 3 illustrates the calibration plots for gallic acid oxidation on TRG modified electrodes recorded in the concentration range from 1 μM to 10 μM (please refer to Figure S4 of Supporting Information for the detailed DPV profiles). Table 2 tabulates the slope, correlation coefficient and peak width at half height ($W_{1/2}$) value for each material. In terms of calibration sensitivity, B-TRG-H exhibited the most sensitive response to oxidation of gallic acid with the highest slope at 0.8610 μA μM^{-1}. With the exception of GC, all the materials showed good linear relationship between peak current and concentration of gallic acid with R^2 values close to one.

Based on the peak width at half height, the selectivity of the materials was evaluated. The materials generally displayed similar selective response toward gallic acid oxidation, where the peak width at half height values fall within the range of 60–70 mV, except that of N-TRG-H exceeding 70 mV.

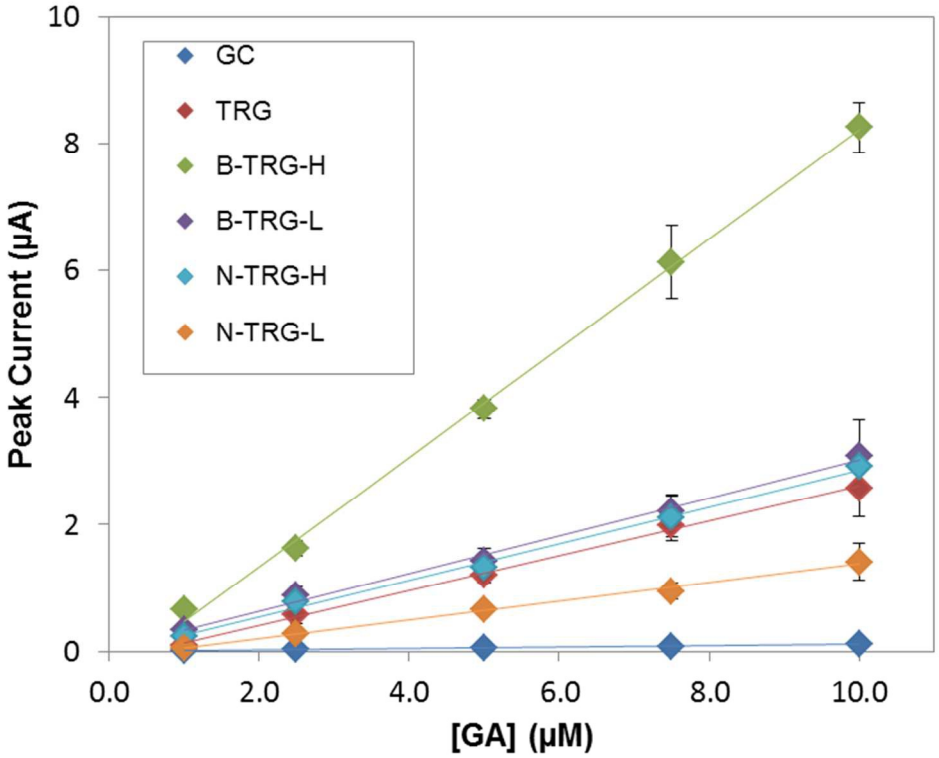

Figure 3. Calibration curves of gallic acid on different materials. Conditions: 0.1 M phosphate buffer solution, pH 2.5.

Table 2. Slope, correlation coefficient and peak width at half height for DPV measurements of gallic acid (concentration range: 1–10 μM) on different materials.

Material	Slope (μA μM^{-1})	R^2	$W_{1/2}$ (mV)
GC	0.0107	0.9773	66
TRG	0.2765	0.9972	68
B-TRG-H	0.8610	0.9983	61
B-TRG-L	0.2971	0.9944	59
N-TRG-H	0.2899	0.9957	79
N-TRG-L	0.1471	0.9957	55

From the analysis of the three analytical parameters, B-TRG-H displayed the most outstanding electroanalytical performance towards the oxidation of standard gallic acid. In order to address the question whether this material could be employed for the analysis of a real sample containing gallic acid, B-TRG-H was used as a sensing platform for the electrochemical detection of gallic acid in tea samples. Such application is important in food science field since it can be adopted to the evaluation of the antioxidant capacity of food and beverages correlated to total polyphenol content.[22]

The analysis of three different tea samples was conducted on B-TRG-H modified electrode. The obtained results from the standard addition method for the analysis of black tea, oolong tea, and green tea samples are consolidated in Table 3. In terms of gallic acid equivalents (GAE), the green tea exhibited the highest antioxidant level, followed by oolong tea and black tea. This result reflects the dissimilar polyphenol content of the three tea samples as expected from the different preparation and fermentation procedures they undergo.[23, 24] Moreover, across the three tea samples, good linear relationship ($R^2 \geq 0.9798$) and reproducibility were acquired.

Table 3. Gallic Acids equivalents (GAE) in tea samples measured by using B-TRG-H as platform. The standard addition method was employed to extrapolate the GAE value from each tea sample. All measurements were performed in 0.1 M phosphate buffer solution, pH 2.5. (GAE = milligrams of gallic acid equivalents per liter).

Tea sample	GAE	RSD (%)	R^2
Black tea	63.80	9	0.9798
Oolong Tea	89.79	13	0.9980
Green Tea	114.18	14	0.9906

In order to ensure the selectivity of the response towards gallic acid in real samples, a study was performed on the concomitant current response of ascorbic acid, which is a non-polyphenol antioxidant also present in several food and beverages containing gallic acid.[25, 26]

With reference to Table S1 and Figure S5 (see Supporting Information), it can be observed that the peak height of gallic acid was unaffected by the increase in concentration of ascorbic acid, being the variation in the signal within the standard deviation obtained for gallic acid detection on the same platform. Furthermore, a significant signal separation of about 280 mV was recorded between gallic acid and ascorbic acid. This confirms the ability of the B-TRG-H-based platform to selectively detect gallic acid in the presence of ascorbic acid. The accuracy of the method was also evaluated by calculating the recoveries upon standard additions of gallic acid to the tea samples. An average recovery value of 97% was obtained, thus indicating minimal effect of matrix interference and demonstrating the suitability of the developed sensor for the application to food analysis.

Conclusion

In summary, we investigated the effect of heteroatom doping on the electrochemical behavior of thermally reduced graphene materials for food science applications. We have found that the type and amount of dopant have a dominant influence on the electrochemical oxidation of gallic acid when compared with other material properties such as such as surface area, density of defects and presence of oxygen functionalities. We observed that the difference in electroactive surface area can explain the results obtained with both nitrogen-doped graphenes and boron-doped graphene containing the lowest amount of dopant. On the other end, doping the graphene material with larger amount of boron infers significantly enhanced performances when compared to nitrogen-doped or undoped materials, due to the thermodynamically favorable electron transfer between gallic acid and the doped graphene, because of the interactions between the electron withdrawing boron and the electron-donating oxygen atoms in

gallic acid. This in turn promotes the gallic acid oxidation and provides a higher peak current on boron-doped graphene.[27]

The boron-doped graphene containing the largest amount of dopant provided the best analytical performance for the detection of gallic acid based on the calibration sensitivity, linearity and selectivity of response. The suitability of a sensing platform based on the best performing boron-doped graphene material, was also demonstrated for the detection of gallic acid in real samples. Three different tea samples were successfully analyzed providing a quantitative evaluation of their antioxidant capacity with minimal matrix interference. Our findings may be significant for the development of graphene-based platforms for the electrochemical detection of biological probes.

Experimental

Equipment

All voltammetric experiments were carried out using a μAutolab type III electrochemical analyzer (Eco Chemie, The Netherlands). All analytical parameters were controlled by General Purpose Electrochemical Systems Version 4.9 software (Eco Chemie, The Netherlands). A three-electrode configuration was employed for the voltammetric measurements in a 8 mL electrochemical cell at ambient temperature. A GC electrode was utilized as a working electrode, a platinum electrode used as an auxiliary electrode and a Ag/AgCl electrode as a reference electrode. For each voltammogram peak current was determined at the potential corresponding to the maximum current.

Materials and methods

Pure graphite microparticles (2– 15 mm, 99.9995 %) were purchased from Alfa Aesar (Singapore). Gallic acid, ascorbic acid, DMF, potassium hydroxide, potassium phosphate dibasic, potassium chloride and sodium chloride were purchased from Sigma–Aldrich (Singapore). Boron trifluoride diethyl etherate (> 46 % BF_3) was obtained from Sigma–Aldrich (Czech Republic). Sulfuric acid (98 %), hydrochloric acid (37 %),

fuming nitric acid (> 98 %), potassium chlorate (99 %), silver nitrate (99.5 %), and barium nitrate (99.5 %) were obtained from Penta (Czech Republic). Nitrogen (99.9999 %) and ammonia (99.9995 %) were obtained from SIAD, Czech Republic. Black tea, Oolong Tea, and Green Tea were obtained from a local supermarket. Glassy carbon electrodes (diameter: 3 mm) were purchased from Autolab (Eco Chemie, The Netherlands). The glassy carbon (GC) electrode was polished with 0.05 μm alumina slurry for renewal of surface.

Preparation of graphite oxide (GO). GO was prepared according to the Staudenmaier method.[28] In brief, nitric acid (9 mL) and sulfuric acid (95–98 %, 17.5 mL) were poured into a flask with stirring at 0 ºC for 15 min. Graphite (1 g) and potassium chlorate (11 g) were added. Following the dissolution of potassium chlorate, the mixture was stirred vigorously for 96 h at ambient temperature. After completion of the reaction, the mixture was added into deionized water (1 L) and filtered. Graphite oxide was then re-dispersed, washed repeatedly in HCl (5 %) solutions and subsequently washed with deionized water until the filtrate was neutralized. Graphite oxide slurry was dried using a vacuum oven at 60 °C for 48 h before use.

*Preparation of undoped thermally reduced graphene (TRG)***.** GO was inserted into a porous quartz-glass capsule connected to a magnetic manipulator in a vacuum tight quartz reactor. The sample was flushed with pure nitrogen for several times and placed in a preheated reactor under nitrogen atmosphere (99.9999 %; pressure: 100 kPa). The sample was thermally exfoliated at 1000 °C for 12 min.

Preparation of B-doped thermally reduced graphene (B-TRG). GO was used as a starting material. The bubbler filled with boron trifluoride diethyl etherate ($BF_3{\cdot}Et_2O$) precursor was used at 20 °C and 1000 mbar. Nitrogen with a flow rate of 100 mL min^{-1} served as a boron-precursor carrier gas and the addition of nitrogen with a flow rate of 1000 mL min^{-1} was used for dilution. The reactor was repeatedly evacuated and flushed with nitrogen. After the flow of boron precursor was stabilized for 5 min, the sample was inserted into the hot zone of the reactor and exfoliated for 12 min at 1000 °C and 800°C.

Preparation of N-doped thermally reduced graphene (N-TRG). GO was used as a

starting material. The quartz–glass reactor was repeatedly evacuated and flushed with nitrogen. The nitrogen flow was switched to ammonia before the sample was transferred to the preheated reactor. The sample was thermally exfoliated for 12 min at 1000 °C and 800 °C.

The desired graphene material with a concentration of 5 mg mL^{-1} in DMF was ultrasonicated (37 kHz) for 5 min before each measurement. Subsequently, the suspension (1 µL) was deposited onto a renewed GC electrode surface and the solvent was evaporated at ambient temperature to give a homogenous TRG layer on the electrode surface.

Scan rate study. The electroactive surface area of GC, TRG, B-TRG-L, B-TRG-H, N-TRG-L, and N-TRG-H was estimated by Randles–Sevcik equation. The peak intensity of 1 mM $K_3[Fe(CN)_6]$ in 0.1 M KCl was measured at different scan rates. The value of diffusion constant was obtained from the literature ($D = 7.2 \times 10^{-6}$ cm^2s^{-1}).[29]

Real sample analysis. Tea solutions were prepared by dissolving 1 teabag into 250 mL of boiling water for 3 min. All the beverage samples were diluted in 0.1 M phosphate buffer solution, pH 2.5. The differential pulse voltammograms were recorded in the range from 0.3 to 0.6 V with 50 ms modulation time and 25 mV modulation amplitude. The concentration of gallic acid was determined by the standard addition method. Results were expressed as milligrams of gallic acid equivalent (GAE) per liter of beverage.

References

1. X. W. Wang, G. Z. Sun, P. Routh, D. H. Kim, W. Huang and P. Chen, *Chem. Soc. Rev.*, 2014, **43**, 7067-7098.

2. M. Pumera, *J. Mater. Chem. C*, 2014, **2**, 6454-6461.

3. R. T. Lv and M. Terrones, *Mater. Lett.*, 2012, **78**, 209-218.

4. Q. Q. Zhu, J. H. Yu, W. S. Zhang, H. Z. Dong and L. F. Dong, *J. Renew. Sustain. Energy*, 2013, **5**.

5. P. Wu, P. Du, H. Zhang and C. X. Cai, *Phys. Chem. Chem. Phys.*, 2013, **15**, 6920-6928.

6. Y. X. Liu, X. C. Dong and P. Chen, *Chem. Soc. Rev.*, 2012, **41**, 2283-2307.

7. L. F. Lai, J. R. Potts, D. Zhan, L. Wang, C. K. Poh, C. H. Tang, H. Gong, Z. X. Shen, L. Y. Jianyi and R. S. Ruoff, *Energy Environ. Sci.*, 2012, **5**, 7936-7942.

8. L. Wang, Z. Sofer, J. Luxa and M. Pumera, *J. Mater. Chem. C*, 2014, **2**, 2887-2893.

9. L. Wang, Z. Sofer, P. Simek, I. Tomandl and M. Pumera, *J. Phys. Chem. C*, 2013, **117**, 23251-23257.

10. P. Lazar, R. Zboril, M. Pumera and M. Otyepka, *Phys. Chem. Chem. Phys.*, 2014, **16**, 14231-14235.

11. Y. H. Lu, Y. Huang, M. J. Zhang and Y. S. Chen, *J. Nanosci. Nanotechnol.*, 2014, **14**, 1134-1144.

12. Z. Yang, H. G. Nie, X. Chen, X. H. Chen and S. M. Huang, *J. Power Sources*, 2013, **236**, 238-249.

13. C. H. Choi, M. W. Chung, H. C. Kwon, S. H. Park and S. I. Woo, *J. Mater. Chem. A*, 2013, **1**, 3694-3699.

14. C. H. Choi, S. H. Park and S. I. Woo, *ACS Nano*, 2012, **6**, 7084-7091.

15. D. W. Wang and D. S. Su, *Energy Environ. Sci.*, 2014, **7**, 576-591.

16. H. L. Poh, P. Simek, Z. Sofer, I. Tomandl and M. Pumera, *J. Mater. Chem. A*, 2013, **1**, 13146-13153.

17. Y. Zhao, L. Yang, S. Chen, X. Wang, Y. Ma, Q. Wu, Y. Jiang, W. Qian and Z. Hu, *J. Am. Chem. Soc.*, 2013, **135**, 1201-1204.

18. S. M. Tan, H. L. Poh, Z. Sofer and M. Pumera, *Analyst*, 2013, **138**, 4885-4891.

19. A. Ambrosi, H. L. Poh, L. Wang, Z. Sofer and M. Pumera, *Chemsuschem*, 2014, **7**, 1102-1106.

20. Z. Zuo, Z. Jiang and A. Manthiram, *J. Mater. Chem. A*, 2013, **1**, 13476-13483.

21. A. Ambrosi, A. Bonanni, Z. Sofer, J. S. Cross and M. Pumera, *Chem. - Eur. J.*, 2011, **17**, 10763-10770.

22. L. P. Souza, F. Calegari, A. J. G. Zarbin, L. H. Marcolino and M. F. Bergamini, *J. Agr. Food Chem.*, 2011, **59**, 7620-7625.

23. H. Panda, *The Complete Book on Cultivation and Manufacture of Tea*, Asia Pacific Business Press Inc., 2011.

24. D. M. Wang, J. L. Lu, A. Q. Miao, Z. Y. Xie and D. P. Yang, *J. Food Comp. Anal.*, 2008, **21**, 361-369.

25. M. D. Pinto, *Food Res. Int.*, 2013, **53**, 558-567.

26. Z. Y. Chen, Q. Y. Zhu, Y. F. Wong, Z. S. Zhang and H. Y. Chung, *J. Agr. Food Chem.*, 1998, **46**, 2512-2516.

27. Y. X. Zhang, J. Zhang and D. S. Su, *Chemsuschem*, 2014, **7**, 1240-1250.

28. L. Staudenmaier, *Ber. Dtsch. Chem. Ges.*, 1898, **31**, 1481-1487.

29. S. J. Konopka and B. McDuffie, *Anal. Chem.*, 1970, **42**, 1741-&.